Monitoring the Concrete Slab Bridge on Balladelaan in the Netherlands using Embedded Ultrasonic Sensors

Hao Cheng, Yuguang Yang, Floris Besseling

Delft University of Technology, Delft, The Netherlands

Coen Kortendijk, Anke Hoekstra

Witteveen+Bos, Deventer, The Netherlands

Contact: h.cheng-2@tudelft.nl

Abstract

The concrete slab bridge on Balladelaan in the Netherlands was built in 1946. It is a cast-in-place concrete bridge with five spans that together form a statically indeterminate deck system. For this type of concrete bridge, shear failure often appears to be the critical failure mechanism, raising concerns about the structural capacity and remaining service life of the bridge. Additionally, the bridge has undergone several undocumented modifications over its lifetime, making it difficult to accurately assess its safety. To monitor this bridge and predict its structural capacity, 22 ultrasonic sensors, known as Smart Aggregates (SAs), and 16 temperature sensors were embedded in the bridge by drilling holes to track changes such as crack development, stress variations, and temperature fluctuations. This paper presents the initial phase measurements from the SAs and temperature sensors in the monitoring project. The main goals of this phase are (1) to ensure that the installed sensors function properly and (2) to establish a preliminary correlation between the measurements from the SAs and the temperature sensors.

Keywords: Concrete slab bridge; Structural health monitoring; Ultrasonics; Smart aggregates.

1 Introduction

Growing concerns about the safety of concrete infrastructure, such as bridges and viaducts, have emerged in the Netherlands. These concerns are primarily driven by three factors: outdated structural designs, material deterioration over time, and increasing traffic volume and weight [1]. Most bridges and viaducts were designed to meet the traffic demands anticipated at the time of their construction. However, these older designs are often insufficient to handle the significantly higher traffic loads specified by modern design codes. This highlights the critical need for reliable structural health monitoring (SHM) techniques to identify structural damage at an early stage. By detecting issues before they escalate into catastrophic failures, SHM systems enable timely maintenance and repairs, which are essential for ensuring the safety of critical concrete infrastructure. The failure of such structures could result in severe consequences, including substantial loss of life and property.

In concrete structures, various indicators can be monitored to evaluate their safety and health. These include global behavioural changes, such as variations in natural frequency [2] and mode shape [3], as well as local changes, such as visible cracks

[4] and changes in strain or stress [5]. Monitoring local changes is particularly important because localized damage, such as shear cracks in shear-critical zones, can lead to global failures. This is especially relevant for short-span concrete bridges [6], where global monitoring alone may fail to detect critical local issues. Consequently, focusing on local behaviour provides a more effective and proactive approach to maintaining structural safety.

To explore the feasibility of long-term monitoring of concrete bridges through local behaviour changes and to promote locally-based monitoring practices in the Netherlands, a concrete bridge built in 1946 on Balladelaan in Amersfoort has been selected as a "living lab" for developing a new SHM system. This slab bridge, typical of post-war construction, uses plain reinforcement bars. For concrete bridges from this era, shear failure is often a critical failure mechanism, raising concerns about the bridge's structural capacity and remaining service life. To track local changes such as crack formation and stress variations, ultrasonic sensors known as Smart Aggregates (SAs) have been embedded within the structure. This paper details the initial phase of the monitoring project, including preparations, sensor installation, and preliminary analyses.

2 The Bridge on Balladelaan in Amersfoort, the Netherlands

The bridge on Balladelaan in Amersfoort was constructed in 1946. It is a cast-in-place concrete slab bridge with five spans, forming a statically indeterminate deck system. The bridge accommodates a bus lane, a cycle path, and a pedestrian path, as shown in Figure 1.

Concrete slab bridges built during the same period as the Balladelaan bridge were typically reinforced with plain rebars of low yield strength in the longitudinal direction. These bridges were primarily designed to resist bending failure, with no shear reinforcement or reliable shear calculations incorporated into their design, as shown in Figure 1(b). As a result, they often lack sufficient shear capacity when evaluated against modern design codes.

Unlike bending failures, which typically exhibit warning signs, shear failures in concrete members without shear reinforcement are brittle and occur suddenly. Upon failure, a critical shear crack initiates from an existing flexural crack inside the bridge deck, making it difficult to detect on the surface. A notable example of such a failure is the collapse of the Weiselburg Bridge in Austria in 2020 [7], as illustrated in Figure 2.

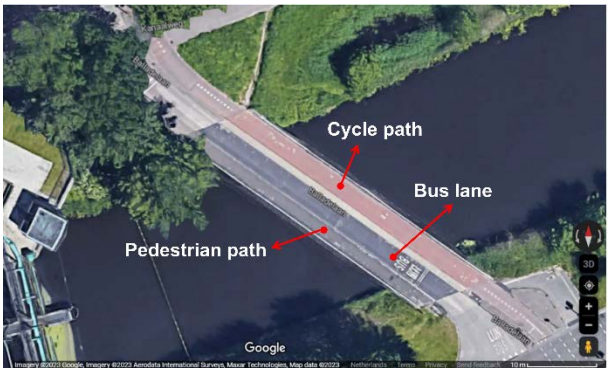

(a) Top view of Balladelaan bridge (source: google.com)

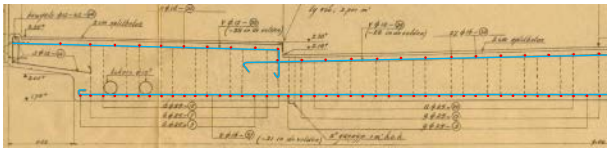

(b) Typical reinforcement layout at the midspan and half-width of the transverse cross-section. Red dots indicate longitudinal reinforcements, while blue lines represent transverse reinforcements.

Figure 1. Balladelaan bridge and reinforcement layout.

Figure 2. Photo of the collapsed Weiselburg bridge and an indication of its failure process [7].

3 Sensors and Monitoring System

3.1 Embeddable Ultrasonic Sensors: Smart Aggregates (SAs)

Smart Aggregates (SAs), first introduced by Song et al. [8], are embeddable piezoelectric sensors designed for the long-term monitoring of concrete structures. A photograph of an SA is shown in Figure 3. These sensors can be embedded within concrete prior to casting in new constructions or installed into drilled holes in existing structures. Leveraging the reversible piezoelectric effect, SAs serve dual functions: they act as actuators to generate high-frequency elastic waves and as receivers to detect these waves within the concrete. This functionality enables SAs, when installed in multiple locations, to monitor crack development across a specified area of the structure.

Compared to other sensor technologies, SAs offer distinct advantages. Fibre optic sensors, such as fibre Bragg gratings [9] and distributed fibre optic sensors [10], are designed to monitor changes at specific points or along the fibre's length. However, SAs function as a network, offering wider coverage within the concrete. Additionally, in comparison to surface-contact piezoelectric sensors like acoustic emission sensors, SAs provide greater durability and reduced sensitivity to environmental variations. These characteristics make SAs especially well-suited for the long-term monitoring of concrete structures [11].

Figure 3. Photo of a Smart Aggregate (SA).

3.2 Temperature Sensors: PT1000 and DS18B20

The bridge was equipped with a total of 16 temperature sensors, 8 PT1000 sensors and 8 DS18B20 sensors, to measure the temperature of the concrete near SAs. This setup aims to account for temperature-induced variations in the elastic waves.

PT1000 sensors are resistance-based devices that require relatively short cables to connect to sensitive analogue-to-digital converters. To facilitate their operation, two 4-channel converters were installed beneath the bridge near the sensors. These converters communicate via a 4G connection.

In contrast, the DS18B20 sensors are digital and can be connected via longer cables. These sensors are linked to a cabinet located at the embankment.

3.3 Monitoring System

The monitoring system comprises a data acquisition (DAQ) system for signals received by the SAs, an ARM embedded board for temperature measurements, and a 4G router with a SIM card for communication. The DAQ system, designed and patented by Delft University of Technology (TU Delft), is optimized for ultrasound-based monitoring of concrete structures.

The DAQ system includes a pulser, pre-amplifiers, and multiplexers. Thanks to the specialized circuit board design, the pulser can generate square pulses with a magnitude of up to 300 V without interfering with the received signals. The system supports a maximum sampling rate of 3 MHz, which is well-suited for the requirements of ultrasound-based concrete monitoring applications.

Figure 4. Photo of the equipment cabinet on the fenced terrain.

4 Sensor Locations

The bridge features three sensor clusters: two at the midspan and one at the edge span. Installation involved drilling 11 holes, labelled Hole A through Hole K, along the bus lane. These holes accommodate SAs and temperature sensors.

Each hole contains two SAs placed along the thickness direction, forming a network to monitor localized changes. Additionally, Holes A, B, C, F, G, I, J, and K each include two temperature sensors installed alongside the SAs, as detailed in Table 1. The vertical distance between the top and bottom SAs in each hole is fixed at 300 mm. The top SAs are consistently positioned 175 mm below the top surface of the bridge slab, while the bottom SAs are set 475 mm below the top surface.

Table 1. Labels for SAs and temperature sensors.

Hole label	SA label		Temperature sensor label		Temperature sensor type
	Top	Bottom	Top	Bottom	
A	306	307	A1	A2	PT1000
B	308	309	B1	B2	DS18B20
C	310	313	C1	C2	DS18B20
D	316	324	-	-	-
E	326	329	-	-	-
F	331	334	F1	F2	DS18B20
G	337	338	G1	G2	PT1000
H	339	340	-	-	-
I	342	344	I1	I2	PT1000
J	347	356	J1	J2	DS18B20
K	359	363	K1	K2	PT1000

The first sensor cluster, located at the midspan, consists of SAs in Holes A through D. These sensors are strategically positioned to detect flexural crack development, which is critical for preventing flexural failure of the bridge. Their exact locations are illustrated in Figure 5. The second cluster, comprising SAs in Holes E through H, is situated at intermediate supports to monitor potential stress changes or crack openings, as shown in Figure 5. The third cluster, located in Holes I through K, is designed to detect the initiation or progression of diagonal cracks in shear-critical zones, as depicted in Figure 6.

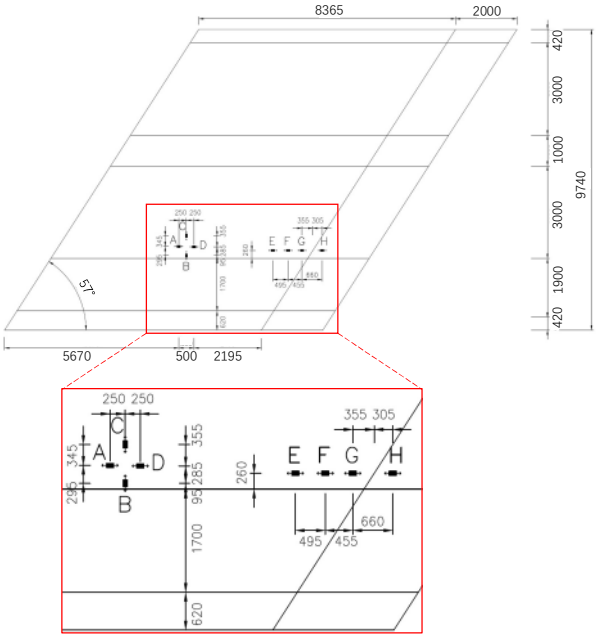

(a) Top view (sensor locations in plane x-y direction).

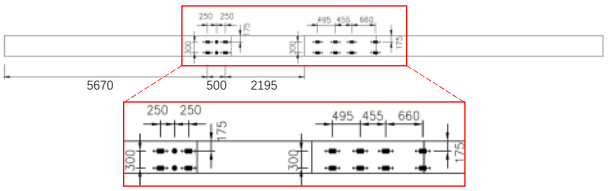

(b) Cross section side view (sensor locations along the thickness direction).

Figure 5. Sensor locations in the midspan (unit: mm).

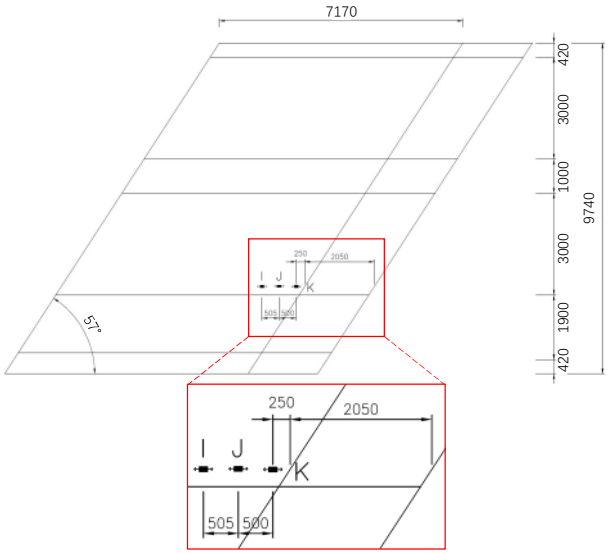

(a) Top view (sensor locations in plane x-y direction).

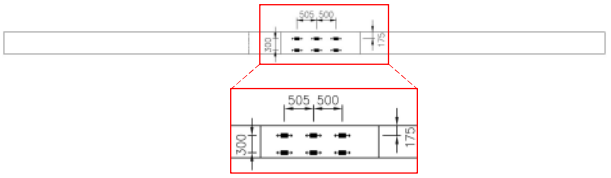

(b) Cross section side view (sensor locations along the thickness direction).

Figure 6. Sensor locations in the edge span (unit: mm).

5 Sensor Installation

The sensor preparation was conducted at TU Delft. SAs were affixed to copper wires using glue to ensure their alignment with the specified orientation and spacing, as illustrated in Figure 7. At select locations mentioned in Section 4, temperature sensors were also glued adjacent to the SAs on the copper wires to measure temperatures in close proximity to the sensor positions, as depicted in Figure 8.

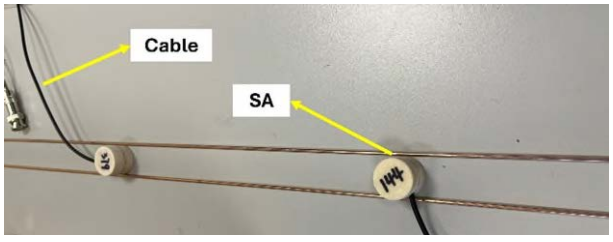

Figure 7. Photo of SAs on the copper wire

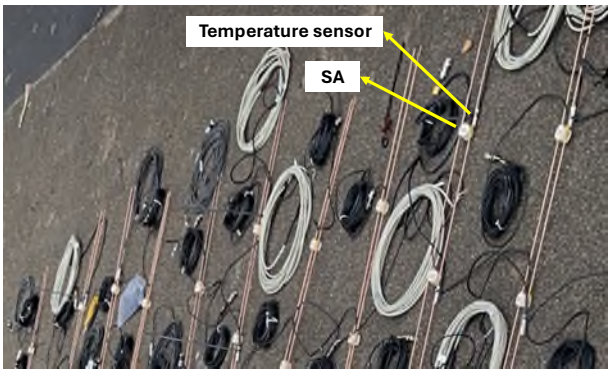

Figure 8. Photo of SAs with temperature sensors.

The entire installation process followed these steps:

- Determining the rebar layout using a radar-based rebar detector.
- Identifying drilling locations based on the rebar layout.
- Drilling holes at the designated sensor locations, as depicted in Figure 9 (a).
- Installing sensors into the drilled holes.
- Filling the holes with high-strength mortar, as demonstrated in Figure 9 (b).
- Installing the data acquisition systems and organizing cables, as shown in Figure 9 (c).
- Installing the main station on the bank.

(a) Designated drilling locations after hole drilling.

(b) Fresh high-strength mortar after hole filling.

(c) Installation of data acquisition systems and Organizing cables.

Figure 9. Photos for the installation process.

6 Preliminary Measurements

6.1 Measurement Data from SA using the DAQ System

The SA measurements are organized into sensor clusters. In a typical measurement, one SA functions as the transmitter while the remaining SAs in the cluster act as receivers. When a measurement begins, the measurement order is assigned remotely, and a high-voltage electric pulse is sent to the transmitter to initiate vibration. This electric pulse is converted into a mechanical wave that propagates through the concrete. Upon reaching the receivers, the wave signals are converted back into electrical signals, recorded as 1D time-series data, and stored locally at the data station. The data acquisition system supports a sampling frequency of up to 3 MHz, enabling the recording of wave signals with frequencies up to 300 kHz without aliasing. Each measurement lasts for 4 ms from the moment the transmitter receives the electric pulse. Both the measurement duration and sampling rate can be adjusted based on signal observations.

In a cluster of *n* SAs, each measurement generates *n*−1 data series. The locally stored wave signals are retrieved remotely to the TU Delft server as needed. Metadata for each measurement includes the naming of time-series data in a format exemplified in Figure 10.

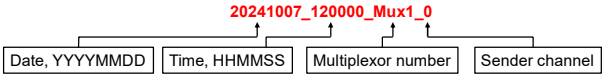

Figure 10. Data file naming.

Figure 11(a) presents a typical measurement obtained from the SAs. To analyse the frequency characteristics, the time-frequency spectrum of the signal is shown in Figure 11(b). The spectrum reveals that the energy is concentrated below 300 kHz, confirming no aliasing occurs. Similar patterns are observed for other sensor pairs but are not displayed here.

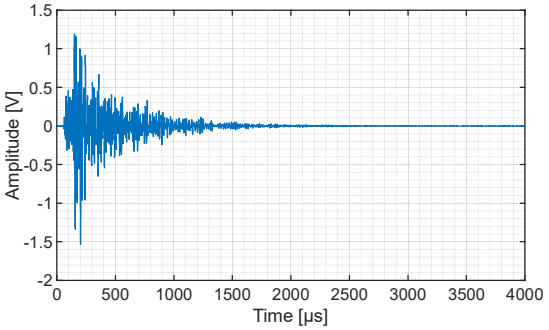

(a) Time domain signal.

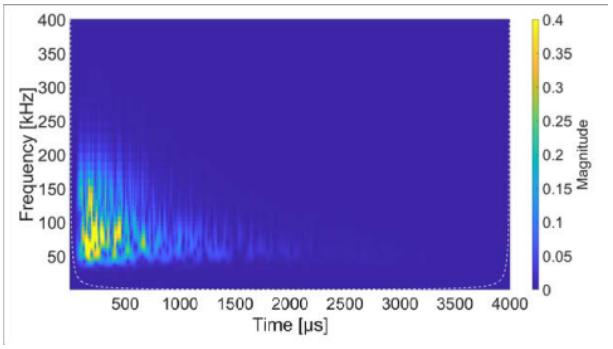

(b) Time-frequency spectrum. The white dashed line indicates the cone of influence (COI), denoting the area where edge effects become significant.

Figure 11. Measurement from the SA pair 306 (transmitter) to 308 (receiver).

As part of the initial data verification, the signal-to-noise ratio and measurement duration were assessed. For signal-to-noise evaluation, the signal from sensor pair 326-340 (Hole E top to Hole H bottom) was analysed. This pair represents the longest distance in the monitoring system at 1637 mm. Based on previous lab tests, wave signals traveling more than 1.5 m are expected to experience significant attenuation. Figure 12 confirms this, showing a maximum signal amplitude of 0.04 V—30 times smaller than that of sensor pair 306-308 (Figure 11(a)). Despite the attenuation, the signal remains clearly distinguishable from the noise level observed before the signal arrival at 300 µs. This result indicates that the monitoring system is sufficiently sensitive to detect even the weakest signals. Additionally, the signal attenuation to the noise level suggests the system's measurement duration is adequate. These findings confirm that the DAQ system design for the SA monitoring system performs as intended.

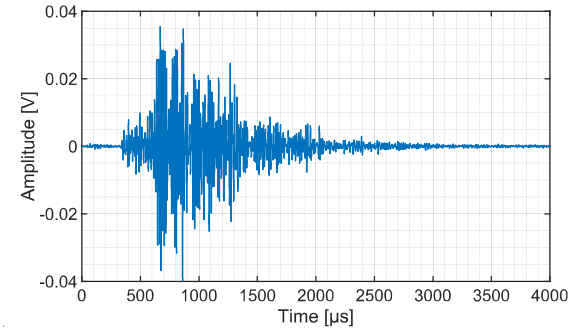

Figure 12. Measurement from the SA pair 326 (transmitter) to 340 (receiver).

6.2 Correlation between Measurements from Smart Aggregates and Temperature Sensors

Preliminary laboratory measurements indicate that wave velocity is a key parameter for identifying variations in the stress level of concrete. However, wave velocity is also highly sensitive to temperature variations in the medium. Therefore, it is essential to first study the influence of temperature on measured wave velocity. To achieve this, three measurements are conducted daily at time slots expected to exhibit the largest temperature differences within a day. The relationship between wave velocity and temperature changes is further analysed in Section 6.2.2.

6.2.1 Signal Processing Technique

Starting from July 6, 2024, the SA system began operating on a regular data acquisition schedule. Under this schedule, three active measurements are performed daily at fixed time slots. The newly acquired wave data are compared with previous measurements to evaluate signal consistency over time and to analyse variations in wave velocity. The data collected up to the time of this report demonstrate that the wave signals remain sufficiently consistent over time, allowing reliable velocity changes to be determined using coda wave interferometry.

The stretching technique [12, 13] is utilized to retrieve the velocity changes. This technique calculates correlation coefficients of windowed signals recorded in an unperturbed state, u_{unp}, and after (or during) the perturbation, u_{per}, in the time domain using [14]:

$$CC(t_c,T,\varepsilon)=\frac{\int_{t_c-T}^{t_c+T} u_{\mathrm{unp}}^{(t_c)}(t)\,u_{\mathrm{per}}^{(t_c)}\left(t(1-\varepsilon)\right)\mathrm{d}t}{\sqrt{\int_{t_c-T}^{t_c+T}\left[u_{\mathrm{unp}}^{(t_c)}(t)\right]^2\mathrm{d}t}\sqrt{\int_{t_c-T}^{t_c+T}\left[u_{\mathrm{per}}^{(t_c)}\left(t(1-\varepsilon)\right)\right]^2\mathrm{d}t}}, \quad (1)$$

where the time window is centred at time t_c with a duration of $2T$ and ε denotes the stretching factor. In case of a uniform velocity change dv in the medium, the stretching factor that maximizes $CC(t_c,T,\varepsilon)$, $\varepsilon_{\mathrm{max}}$, coincides with the relative change in travel time, dt/t.

6.2.2 Comparison between SA and Temperature Sensor Measurements

Figure 13 presents a preliminary correlation between velocity changes observed in the SA pair 306-308 (with SA 306 as the transmitter) and temperature readings from sensor A1. The results suggest a consistent relationship between the two sensor types. Future work will involve correlating all SA measurements with temperature data to further analyse the temperature-induced changes in wave velocity.

Once the effects of temperature on wave velocity are understood, further investigations will focus on stress-induced or crack-induced velocity changes, isolating them from temperature-related effects. It is also important to note that temperature changes across the thickness of the bridge deck can lead to a stress gradient at different times of the day. This delayed thermal effect requires further investigation as additional data become available.

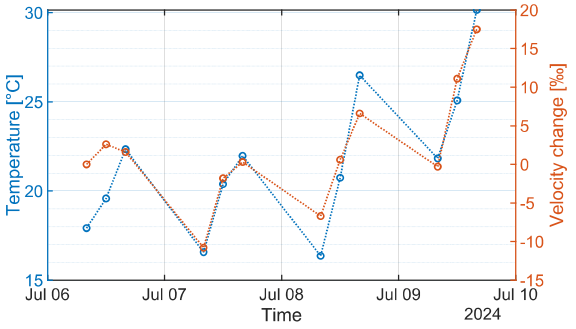

Figure 13. Correlation between SA pair 306-308 (with 306 as the transmitter) and the temperature sensor A1.

7 Follow-up Assessment of Existing State based on Load Tests

The next phase focuses on further structural identification of the bridge and assessing its current condition through load testing. This involves driving a test vehicle of known weight over the bridge to calibrate the SA measurements against known loads.

In this test, a vehicle with predetermined axle loads will be positioned at critical locations on the bridge deck. These critical locations are identified through structural analysis using linear finite element modelling (FEM) with updated bridge deck geometry and material properties. This test will provide the first attempt to correlate SA measurements with stress changes caused by the vehicle load. The results will be compared with FEM predictions to validate the measurement approach. This process is key to understanding load transfer mechanisms within the bridge and evaluating the response of the SAs to specific loads. Repeating such load tests in the future can help track variations in the structural response of the SAs under identical loading conditions, which can serve as a performance indicator for the bridge's condition over time.

As a potential additional step, Acoustic Emission (AE) measurements may be conducted during the load test. It is anticipated that when the vehicle's weight is sufficiently high, existing cracks in the bridge deck may reopen, generating AE signals, particularly during unloading. This technique can help detect and locate existing (shear) cracks within the concrete that are not visible externally.

8 Conclusions

Based on the findings to date, the following conclusions can be made:

- The monitoring system, including the temperature sensors and SAs, is performing as expected.
- The selected measurement duration and sensor spacing are appropriate, resulting in high-quality signals with a high signal-to-noise ratio.
- Temperature significantly influences the extracted wave velocities, and this effect must be accounted for or corrected in future measurements to accurately estimate stress-induced velocity changes.

9 References

[1] Rijkswaterstaat, Inventarisatie Kunstwerken. *Brief aan de Voorzitter* **2007**.

[2] Salawu, O. S., Detection of structural damage through changes in frequency: a review. *Engineering structures* **1997,** 19, (9), 718-723.

[3] Fayyadh, M. M.; Abdul Razak, H., Detection of damage location using mode shape deviation: Numerical study. *International Journal of Physical Sciences* **2011,** 6, (24), 5688-5698.

[4] Golewski, G. L., The phenomenon of cracking in cement concretes and reinforced concrete structures: the mechanism of cracks formation, causes of their initiation, types and places of occurrence, and methods of detection—a review. *Buildings* **2023,** 13, (3), 765.

[5] Jiang, H. W.; Zhang, J. Q.; Jiang, R. N., Stress Evaluation for Rocks and Structural Concrete Members through Ultrasonic Wave Analysis: Review. *Journal of Materials in Civil Engineering* **2017,** 29, (10), 10.

[6] Sierra, P. L.; Poliotti, M.; Yang, Y.; García, X. M.; Chacón, R. In *Dynamic Characterization of a Real-Scale Prestressed Concrete Beam Tested Until Failure*, International Symposium of the International Federation for Structural Concrete, 2023; Springer: 2023; pp 896-906.

[7] Huber, T.; Kollegger, J.; Suza, D.; Huber, P., The Wieselburg Bridge collapse—Analysis of the shear capacity based on forensic data. *Structural Concrete* **2024,** 25, (4), 2784-2799.

[8] Song, G. B.; Gu, H. C.; Mo, Y. L., Smart aggregates: multi-functional sensors for concrete structures - a tutorial and a review. *Smart Materials and Structures* **2008,** 17, (3), 17.

[9] Ho, S. C. M.; Ren, L.; Labib, E.; Kapadia, A.; Mo, Y. L.; Li, H.; Song, G., Inference of bond slip in prestressed tendons in concrete bridge girders. *Structural Control and Health Monitoring* **2015,** 22, (2), 289-300.

[10] Bao, Y.; Valipour, M.; Meng, W.; Khayat, K. H.; Chen, G., Distributed fiber optic sensor-enhanced detection and prediction of shrinkage-induced delamination of ultra-high-performance concrete overlay. *Smart Materials and Structures* **2017,** 26, (8), 085009.

[11] Cheng, H.; Zhang, F.; Yang, Y.; Blom, C. B. M., Monitoring of Repaired Concrete Floor in the Maastunnel using Smart Aggregates. In *Bridge Maintenance, Safety, Management, Life-cycle Sustainability and Innovations*, 2022.

[12] Lobkis, O. I.; Weaver, R. L., Coda-wave interferometry in finite solids: recovery of P-to-S conversion rates in an elastodynamic billiard. *Phys Rev Lett* **2003,** 90, (25 Pt 1), 254302.

[13] Sens-Schönfelder, C.; Wegler, U., Passive image interferometry and seasonal variations of seismic velocities at Merapi Volcano, Indonesia. *Geophys. Res. Lett.* **2006,** 33, (21), 5.

[14] Cheng, H.; Weemstra, C.; Hendriks, M. A. N.; Yang, Y., Comparing the stretching technique and the wavelet cross-spectrum technique for measuring stress-induced wave-velocity changes in concrete. *Autom. Constr.* **2024,** 158, 105221.